



Article

# Early Detection of Plant Physiological Responses to Different Levels of Water Stress Using Reflectance Spectroscopy

Matthew Maimaitiyiming <sup>1,2,\*</sup> , Abduwasit Ghulam <sup>1,2,\*</sup>, Arianna Bozzolo <sup>3</sup>, Joseph L. Wilkins <sup>2,4</sup>  and Misha T. Kwasniewski <sup>3</sup>

<sup>1</sup> Center for Sustainability, Saint Louis University, St. Louis, MO 63108, USA

<sup>2</sup> Department of Earth and Atmospheric Sciences, Saint Louis University, St. Louis, MO 63108, USA; wilkins.joseph@epa.gov

<sup>3</sup> Grape and Wine Institute, University of Missouri, 221 Eckles Hall, Columbia, MO 65211, USA; arianna.bozzolo@cbrands.com (A.B.); kwasniewskim@missouri.edu (M.T.K.)

<sup>4</sup> Computational Exposure Division, National Exposure Research Laboratory, Office of Research and Development, U.S. Environmental Protection Agency, Durham, NC 27711, USA

\* Correspondence: maimaitiyiming@slu.edu (M.M.); awulamu@slu.edu (A.G.); Tel.: +1-314-977-5156 (A.G.)

Academic Editors: Lenio Soares Galvao, Clement Atzberger and Prasad S. Thenkabail

Received: 23 March 2017; Accepted: 13 July 2017; Published: 19 July 2017

**Abstract:** Early detection of water stress is critical for precision farming for improving crop productivity and fruit quality. To investigate varying rootstock and irrigation interactions in an open agricultural ecosystem, different irrigation treatments were implemented in a vineyard experimental site either: (i) nonirrigated (NIR); (ii) with full replacement of evapotranspiration (FIR); or (iii) intermediate irrigation (INT, 50% replacement of evapotranspiration). In the summers 2014 and 2015, we collected leaf reflectance factor spectra of the vineyard using field spectroscopy along with grapevine physiological parameters. To comprehensively analyze the field-collected hyperspectral data, various band combinations were used to calculate the normalized difference spectral index (NDSI) along with 26 various indices from the literature. Then, the relationship between the indices and plant physiological parameters were examined and the strongest relationships were determined. We found that newly-identified NDSIs always performed better than the indices from the literature, and stomatal conductance ( $G_s$ ) was the plant physiological parameter that showed the highest correlation with  $NDSI(R_{603}, R_{558})$  calculated using leaf reflectance factor spectra ( $R^2 = 0.720$ ). Additionally, the best  $NDSI(R_{685}, R_{415})$  for non-photochemical quenching (NPQ) was determined ( $R^2 = 0.681$ ).  $G_s$  resulted in being a proxy of water stress. Therefore, the partial least squares regression (PLSR) method was utilized to develop a predictive model for  $G_s$ . Our results showed that the PLSR model was inferior to the NDSI in  $G_s$  estimation ( $R^2 = 0.680$ ). The variable importance in the projection (VIP) was then employed to investigate the most important wavelengths that were most effective in determining  $G_s$ . The VIP analysis confirmed that the yellow band improves the prediction ability of hyperspectral reflectance factor data in  $G_s$  estimation. The findings of this study demonstrate the potential of hyperspectral spectroscopy data in monitoring plant stress response.

**Keywords:** grapevine; water stress; stomatal conductance; leaf reflectance factor; NDSI; PLSR

## 1. Introduction

One of the significant impacts of climate change due to rising temperatures is alteration in water supply and demand for the plant communities, which are a critical source of food [1]. It has been long recognized that the lack of water availability has an adverse effect on the plant growth process, thus

decreasing crop productivity and yield [2]. Therefore, studies focusing on early detection and warning of plant water stress are of considerable significance.

Grapevine (*Vitis* spp.) is considered the most commercially-important berry crop in the world [3]. North American *Vitis* species play a vital role in the global grape industry by imparting important pest resistance through their use as rootstocks (the below-ground part makes up the lower stem and roots), their contributions to hybrid scions (the above-ground part of the plant; the scion produces the stem, leaves, flowers and berries) or through planting as an ungrafted plant. Today, grape growing is emerging as a more important part of rural agriculture in the Midwestern United States. For instance, in Missouri, the economic impact of grapes and wine has grown to be worth \$1.6 billion with a 16% annual growth rate [4]. However, abiotic and biotic stresses are restrictive factors impacting cultivation of even the grafted *V. vinifera* ssp. *Vinifera* and hybrid scions derived from crosses between *V. vinifera* ssp. *vinifera* and one of the native North American *Vitis* species are dominant cultivated grapevines in the Midwest. Moreover, fruit quality and yield will be significantly affected by prolonged drought, which is projected in the Midwestern United States [5].

The severity and duration of a plant's dehydration determines the impact of water stress on the photosynthetic performance of the plant and whether or not a plant can recover from stress damage when irrigated. In the short term, water stress causes stomata closure, which in turn not only leads to leaf temperature increase by reducing the transpiration rate, but also creates a reduction in CO<sub>2</sub> concentration [6,7]. If there is an imbalance between the absorbed light energy and the energy requirement for carbon fixation, promoted by stomata closure, this may cause over-excitations and subsequent the photodamage to photosystem II (PSII) reaction centers [8]. As a result, the maximum quantum efficiency of PSII will decline in response to the onset of water stress [9]. When plant stress severity or duration exceeds a critical threshold, plants manifest biochemical and morphological symptoms as adaption strategies. Some adaptation strategies include reduction in chlorophyll content, leaf area, premature leaf senescence and stunted growth [10,11]. In general, if the stressor is removed before the damage is visible to the naked eye, plants revive and develop a new physiological standard [12].

Compared to traditional field measurements, remote sensing can provide timely and reliable information about the current plant physiology in a cost-effective and timely manner [13]. In particular, optical remote sensing exploits reflected radiation in the visible (VIS, 400–700 nm), the near-infrared (NIR, 700–1200 nm) and short-wave-infrared (SWIR, 1300–2500 nm) regions of electromagnetic spectrum recorded with use of ground, air- and space-borne sensors. Generally, these regions are strongly correlated with leaf pigment concentration, cell structure and water content, respectively [14–18]. The reflectance data recorded with remote sensors are often used to calculate vegetation indices (VIs), which are a mathematical combination of several bands within the visible and NIR spectral regions. VIs have been proven to be a very simple yet effective approach in estimating biophysical variables [19–21]. Narrow band hyperspectral remote sensors, unlike broad band multispectral remote sensors, record reflected radiant energy from the objects at a high number of wavebands, and VIs calculated from hyperspectral data provided new insights into the early detection of plant stress [22–25]. The photochemical reflectance index (PRI), originally designed for epoxidation state of the xanthophyll cycle pigments, is an example promising narrow band index that can detect non-photochemical quenching, one of the two photo-protective mechanisms [24]. Sun-induced fluorescence (SIF) emission is another alternative photo-protective mechanism that minimizes the damages to the photosystem by re-emitting the excess absorbed light energy as fluorescence [26]. In recent years hyperspectral sensors have demonstrated the feasibility of SIF retrieval at multiple scales and confirmed further possibilities to detect plant stress before it is visible to the naked eye [27–32].

Recent studies demonstrated that normalized difference spectral indices (NDSI) using all possible combination of two bands outperformed previously-published indices for prediction of biochemical, biophysical and structural plant parameters [33–40]. Additionally, two-dimensional visualization of coefficient of determination ( $R^2$ ) between NDSIs and biophysical variables provide a clear overview

of effective wavebands and spectral regions for determining optimal normalized indices to predict various parameters under study [35]. On the other hand, partial least squares regression (PLSR) has been frequently used for band selection analysis at the leaf and canopy levels [41,42]. PLSR reduces collinearity that commonly exists in hyperspectral data by producing non-correlated, statistically independent latent factors that are a linear combination of the original spectral bands. Both the spectral information and the dependent variables are given equal consideration when latent vectors are regressed against the dependent variable using a cross-validated linear model. The advantages of PLSR approach include: (1) it utilizes the continuous spectrum rather than in a band-by-band type of analysis [43,44]; and (2) statistical over-fitting can be minimized by defining the number of orthogonal latent vectors that produces the smallest root mean square error in cross-validation [45].

The primary objectives of this study were to: (1) investigate the potential of field spectroscopy for characterizing the physiological status of grapevines exposed to different levels of water stress based on in situ measurements; and (2) identify the most effective indices and predictive models for early detection of plant response to water stress using the NDSI and PLSR approaches.

## 2. Materials and Methods

### 2.1. Study Site

Field data collection was carried out in a vineyard situated in Mount Vernon, MO, USA (37°4'27.17''N, 93°52'46.70''W, altitude 376 m) during the growing seasons of 2014 and 2015 (Figure 1). The region has a continental climate with an average annual temperature of 15.6 °C and mean annual rainfall of 1066.8 mm. The vineyard was established on 25 June 2008 to investigate varying rootstocks and irrigation interactions in tandem. At establishment, six irrigation zones were installed allowing for randomization of blocks for both three different irrigation regimes and four different rootstocks. Chambourcin vines, either own-rooted or grafted onto 1103 Paulsen, 3309 Couderc and Selection Oppenheim 4 (SO4) were planted with varying irrigation patterns of either: (i) nonirrigated (NIR); (ii) full replacement of evapotranspiration (FIR); or (iii) intermediate irrigation (INT, 50% replacement of potential evapotranspiration). The vine density was 504 vines ha<sup>-1</sup> with 3 m × 3 m row spacing, including 25 rows and 1034 vines in total. The soil texture was a combination of sandy loam, silt loam and loam, with an average pH of 6. Each vine row was oriented in the east to west direction, and the vines were trained with a high wire cordon trellis and spur pruned. To avoid soil erosion, grass was sown between the rows with a weed free strip maintained just below the vines. Vine rows were numbered from the north and plants were numbered from the west. Originally, the entire field received irrigation at a rate necessary to replace evapotranspiration (ET) until the 2014 season. In the 2014 season, the treatments were initiated, and data collection on the vine water status and fruit quality began.

This study's field measurements involved 9 total rows, Numbers 8–16, where the different irrigation treatments were applied. Each row consisted of 8 plots and 4 vines in each plot with the same rootstocks. For measurement purposes, the third vine from the east side of the plot was chosen. FIR and INT rows were irrigated using a drip irrigation system. To maintain the different treatments during the growing season, both timing and amount of water were determined based on ET calculated from the weather data obtained from a weather station adjacent to the vineyard. The start dates of the treatments were 14 July 2014 (Day of Year: DOY 195) and 1 September 2015 (DOY 244). The end dates were 3 October 2014 (DOY 276) and 9 October 2015 (DOY 282), respectively. Daily average precipitation, maximum and minimum air temperature and precipitation are presented in Figure 2 together with field data collection dates for two study years.

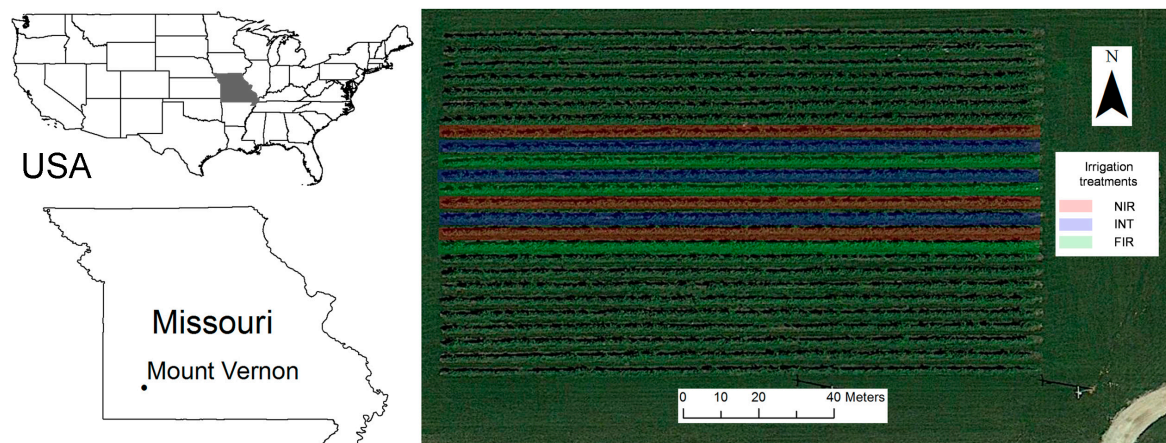


**Figure 1.** Overview of the vineyard used for the experiment in the present study (source: Google Earth). NIR, nonirrigated; FIR, full replacement of evapotranspiration; INT, 50% replacement of evapotranspiration.

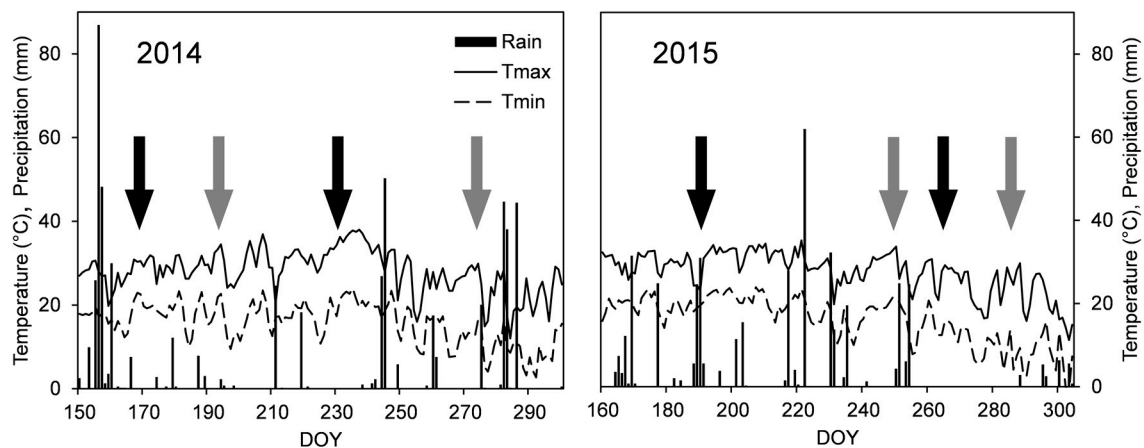


**Figure 2.** Daily average minimum ( $T_{min}$ , °C), maximum air temperature ( $T_{max}$ , °C) and amount of daily precipitation (mm) events. Dark arrows indicate the dates on which field measurements were conducted and gray arrows indicate the start and end dates of irrigation.

## 2.2. Field Data Collection

In the years 2014 and 2015, we collected plant physiological and nutritional variables of the vineyard along with leaf spectra using field spectroscopy. The data collection dates were during early fruit set stage (18 June, DOY 169) and late veraison stage (19 August, DOY 231) in 2014 and during berry touch (10 July, DOY 191) and fruit ripening stage (21 September, DOY 264) in 2015. On these measurement days, no clear damages caused by water stress were identified on grapevine leaves.

### 2.2.1. Plant Physiological Measurements

Midday leaf physiological status was determined using an LI-6400XT Portable Photosynthesis system coupled with a pulse amplitude-modulated (PAM) leaf chamber fluorometer at incident photosynthetic photon flux density (PPFD) level of  $1000 \mu\text{mol m}^{-2} \text{s}^{-1}$  generated by a red LED array, with an additional 10% blue light to maximize stomatal opening (Li-Cor, Inc., Lincoln, NE, USA). Measurements were made on a fully-expanded sunlit leaf on the south-facing side of the vine in each plot for gas exchange and fluorescence variables: stomatal conductance ( $G_s$ ), photosynthetic  $\text{CO}_2$  assimilation rate ( $A_i$ ), chlorophyll fluorescence, electron transport rate (ETR), photochemical ( $qP$ )



and non-photochemical quenching (NPQ) during midday (1000–1500 h) under full sun conditions. Inside the leaf chamber, the CO<sub>2</sub> concentration was set at 400 µmol CO<sub>2</sub> mol<sup>−1</sup> air in the cuvette, and the relative humidity of the incoming air ranged between 40 and 60%; temperature and water vapor pressure deficit (VPD) were not controlled. The chlorophyll fluorescence ( $\Delta F/F_{m'}$ , also known as instantaneous photochemical efficiency of PSII) was calculated as  $(F_{m'} - F_s)/F_{m'}$ , where  $F_{m'}$  is the fluorescence yield and  $F_s$  the steady-state fluorescence of the light-acclimated leaf [46].

### 2.2.2. Hyperspectral Reflectance Measurements

Reflectance factor data of vine leaves, specifically hemispheric conical reflectance factor (HCRF; [47]), were obtained using a Spectral Evolution portable spectroradiometer PSR-3500 (Spectral Evolution, Inc., Lawrence, MA, USA). The spectroradiometer records spectral information of a target in full wavelength range (350–2500 nm) with a resolution of 3.5 nm in the 350–1000 nm range, 10 nm in the 1000–1900 nm range and 7 nm in the 1900–2500 nm range. The spectroradiometer was equipped with a specifically developed leaf clip for the bifurcated fiber-optic connected to both the device and a 5-watt tungsten halogen lamp light source. With the leaf clip, we collected the reflectance factor of the same leaf used for photosynthetic measurements. This combination is useful for acquiring the leaf hemispherical reflectance factor with a spectrally black background after a spectrally white background on the opposite side of the clip was measured for the reference spectrum. The black background measurements were taken three times at different points avoiding leaf veins, and the averaged leaf reflectance factor was used for further analysis.

We used Getac® PS336 PDA preloaded with DARWin software (Compact V.1.2.4903, Spectral Evolution, Inc., Lawrence, MA, USA) to manipulate the spectroradiometer and collect data efficiently in the field. The spectroradiometer was configured to average 40 spectra automatically per sampling, and the raw spectra bandwidth was interpolated to 1 nm. This resulted in 2151 individual spectral bands.

In addition to plant physiological and reflectance measurements, manual harvesting was carried out on 5 October 2014 (DOY 278) and 11 October 2015 (DOY 284), respectively, and the berry weight measurements were determined on-site for each individual vine within the plots.

## 2.3. Methods

### 2.3.1. Selection of Spectral Indices and Sensitive Bands

One of the approaches to explore the significant relationships between plant physiological parameters and hyperspectral data is conducting a comparative analysis of simple normalized difference spectral indices (NDSI) calculated from narrow band reflectance factor spectra. We identify the wavelengths or normalized indices (Equation (1)) that are capable of estimating physiological parameters such as  $G_s$ .

We applied NDSI to identify optimal wavelengths and/or indices. The NDSI is defined as:

$$NDSI(i, j) = \frac{R_i - R_j}{R_i + R_j}, \quad (1)$$

where  $R$  is the reflectance factor value, and the subscripts are wavelengths in nanometer (nm).

NDSIs were calculated for the measured leaf hyperspectral reflectance factor spectra using all possible combinations of available bands ( $i$  and  $j$  nm) in the full spectral region (350–2500 nm), excluding the 1350–1450 nm, 1800–2000 nm and 2300–2500 nm regions due to strong atmospheric H<sub>2</sub>O and CO<sub>2</sub> absorption. Here, we examine the linear relationship between in situ physiological parameters and NDSIs and 2-dimensional maps of coefficient of determination ( $R^2$ ). The  $R^2$  maps allow the evaluation of the different band combinations and the selection of a sensitive NDSI for each physiological parameter under study [35,39,40]. The performance of identified NDSIs was then compared with previously-published indices from the relevant literature as shown in Table 1. The most effective NDSIs and the indices from the literature were determined using  $R^2$  and root mean square

error of calibration ( $RMSE_{cal}$ ) on the randomly-selected calibration dataset (80% of samples,  $n = 169$ ). The predictive ability the indices was evaluated using  $R^2$  and  $RMSE_{val}$  on the independent validation dataset (20% of samples,  $n = 42$ ).

**Table 1.** Spectral indices used in this study.

Reflectance Index	Acronym	Equation	References
<b>Leaf pigment</b>			
Anthocyanin (Gitelson)	Ant <sub>Gitelson</sub>	$Ant_{Gitelson} = (1/R_{550} - 1/R_{700}) \times R_{780}$	[48]
Carotenoid Reflectance Index	CRI1	$CRI1 = 1/R_{510} - 1/R_{550}$	[49]
Carotenoid Reflectance Index	CRI2	$CRI2 = 1/R_{510} - 1/R_{700}$	[49]
Chlorophyll Index	CI	$CI = (R_{750} - R_{705})/(R_{750} + R_{705})$	[50]
Optimized Soil-Adjusted Vegetation Index	OSAVI	$OSAVI = (1 + 0.16) \times (R_{800} - R_{670})/(R_{800} + R_{670} + 0.16)$	[51]
Red Green Index	RGI	$RGI = R_{690}/R_{550}$	[52]
Structure Intensive Pigment Index	SIPI	$SIPI = (R_{800} - R_{450})/(R_{800} + R_{650})$	[53]
Transformed Chlorophyll Absorption in Reflectance Index	TCARI	$TCARI = 3 \times ((R_{700} - R_{670}) - 0.2 \times (R_{700} - R_{550}) \times (R_{700}/R_{670}))$	[54]
	TCARI/OSAVI	TCARI/OSAVI	[54]
Normalized Pigment Chlorophyll Index	NPCI	$NPCI = (R_{680} - R_{430})/(R_{680} + R_{430})$	[55]
<b>Greenness</b>			
Enhanced Vegetation Index EVI	EVI	$(2.5(R_{782} - R_{675})/(R_{782} + 6 \times R_{675} - 7.5 \times R_{445} + 1))$	[56]
Normalized Difference Vegetation Index	NDVI	$NDVI = (R_{800} - R_{670})/(R_{800} + R_{670})$	[57]
Greenness Index	GI	$GI = R_{554}/R_{677}$	[52]
Green NDVI	GNDVI	$GNDVI = (R_{750} - R_{540} + R_{570})/(R_{750} + R_{540} - R_{570})$	[58]
Red Edge Inflection Point	REIP	$REIP = 700 + 40 \times \{[(R_{670} + R_{780})/2 - R_{700}]/(R_{740} - R_{700})\}$	[59]
Simple Ratio	SR	$SR = R_{900}/R_{680}$	[57]
Triangular Vegetation Index	TVI	$TVI = 0.5 \times (120 \times (R_{750} - R_{550}) - 200 \times (R_{670} - R_{550}))$	[60]
<b>Stress</b>			
Fluorescence Ratio Index 1	FRI <sub>1</sub>	$FRI1 = R_{690}/R_{600}$	[61]
Fluorescence Ratio Indices 2	FRI <sub>2</sub>	$FRI2 = R_{740}/R_{800}$	[61]
Modified Red Edge Simple Ratio Index	mRESR	$mRESR = (R_{750} - R_{445})/(R_{705} + R_{445})$	[20]
Normalized Phaeophytinization Index	NPQI	$NPQI = (R_{415} - R_{435})/(R_{415} + R_{435})$	[62]
Photochemical Reflectance Index	PRI	$PRI = (R_{531} - R_{570})/(R_{531} + R_{570})$	[24]
Plant Senescence Reflectance Index	PSRI	$PSRI = (R_{680} - R_{500})/R_{750}$	[63]
Red-Edge Vegetation Stress Index	RVSI	$0.5(R_{722} + R_{763}) - R_{733}$	[64]
Simple Ratio Pigment Index	SRPI	$SRPI = R_{430}/R_{680}$	[65]
<b>Water</b>			
Water Index	WI	$WI = R_{900}/R_{970}$	[66]

### 2.3.2. Multivariate Method

The partial least squares regression (PLSR) is a multivariate regression method that specifies a linear relationship between a set of dependent (response) variables,  $Y$ , and a set of predictor variables,  $X$  [67]. It is a powerful tool specifically designed to deal with the data consisting of many independent variables and is used to reduce collinearity within the data to non-correlated latent variables or factors [68–70]. To select the optimum number of factors and avoid overfitting, we calibrated the model by an iterative leave-one-out cross-validation criterion called the minimum predicted residual sum of squares (PRESS)  $RMSE_{cal}$ .  $RMSE_{cal}$  is minimized by iteratively leaving one sample out of the calibration dataset and calibrating the model from the remaining dataset. To further evaluate the significance of each wavelength for model prediction, variable importance of projection (VIP) values were calculated [71]. The higher the VIP value of a wavelength is, the greater its contribution to the model becomes. Thus, the wavelengths with VIP-values greater than 1 are the most influential predictors in a model. The predictive ability of the best selected PLSR model was assessed using the  $R^2$  and  $RMSE_{val}$  on the independent validation dataset.

### 2.3.3. Sensitivity Analysis for Early Stress Detection

As mentioned in the Introduction section, water stress symptoms in the early stage are not visible. To avoid yield loss, the stress factor must be removed before irreversible damage occurs. Therefore, it is important to test the capability of newly-identified NDSI and the PLSR model for early stress detection. To evaluate the sensitivity of the best selected NDSI model and the PLSR model to the induced water stress based on field measured physiological data, a one-way analysis of variance (ANOVA) followed by an honest significant difference (HSD) Tukey test ( $\alpha = 0.05$ ) was performed to determine significant differences between predicted plant physiological parameters corresponding to the observed different stress levels. Since there were three irrigation treatments (NIR, INT and FIR) intended to induce different levels of water stress within the vineyard, we represented physiological status of grapevine treated with INT irrigation as the early stage of water stress.

### 2.3.4. Statistical Analyses

One-way analysis of variance (ANOVA) was used to investigate the effect of irrigation treatments on the field measured plant physiological parameters. Significant differences between treatments were assessed with HSD Tukey tests ( $\alpha = 0.05$ ). Pearson correlation coefficients were used to explore the significant relationships between plant physiological parameters. All data analyses were performed using IBM SPSS Version 24.0 (SPSS Inc., Chicago, IL, USA).

## 3. Results

### 3.1. Vineyard Weather Condition and Physiological Responses of Grapevines to Induced Water Stress

The average air temperature was higher by 1.7 °C in 2014 for the period covering the stress initiation through the second field measurement date (DOY 195–DOY 231) compared to the same period in 2015 (DOY 244–DOY 264). There was only one >20-mm rain event that occurred during this deficit irrigation period in 2014. In 2015, however, there were two >20-mm events. In both years, there were nine no-rain days prior to the second field measurement date.

In 2014, the mean values of leaf-level physiological parameters were generally lower on 19 August (DOY 231) than the mean values on 18 June (DOY 169), although there were rainfall events during the deficit irrigation period (Table 2). On 19 August, as expected, INT and NIR treatments showed significantly lower photosynthetic activities than the FIR treatment except for the  $qP$ , but the photosynthetic differences between INT and NIR treatments were not significant. Regarding the 2015 data,  $G_s$  decreased for all treatments on 21 September (DOY 264) compared to  $G_s$  on 10 July (DOY 191), yet the differences between treatments were not significant. Despite the irrigation treatment and nine no rain days prior to the measurement date, INT and NIR treatments closely followed the photosynthesis levels of the FIR treatment on 21 September (Table 2). The relationship between  $A_i$  and  $G_s$  was consistent in both study years, and the relationship was stronger during the deficit irrigation period ( $r = 0.82$ ,  $p < 0.01$  for 19 August 2014;  $r = 0.76$ ,  $p < 0.01$  for 21 September 2015). Physiological parameters that showed significant correlation with  $A_i$  were  $F_s$ ,  $F_m'$ ,  $\Delta F/F_m'$ ,  $ETR$  and  $NPQ$ , but these relationships were not consistent in both years (Table 3). Failing to induce different levels of water stress in 2015 did not affect the results of this work, as the purpose of the study was to find the best indicator of water stress, not differentiating levels of water stress. In particular, we selected  $G_s$  as the water stress indicator because it is considered an important parameter to assess water stress by Flexas et al. (2002a) [72], and stomata respond to water stress before there is a detectable change in the leaf water potential and/or leaf water content [73,74].

Across the seasons, berry yield was higher in 2014 (14.51 kg/vine) than in 2015 (14.21 kg/vine), but the difference was not statistically significant ( $p > 0.05$ ). Irrigation only affected the yield in 2014 and there was a significant ( $p < 0.05$ ) difference between the FIR (13.82 kg/vine) and INT (15.70 kg/vine) treatments.

**Table 2.** Grapevine physiological parameters as a function of the irrigation treatments in 2014. Values indicate the mean and pooled RMSE of the ANOVA test.  $G_s$ : stomatal conductance ( $\text{mol H}_2\text{O m}^{-2} \text{s}^{-1}$ );  $A_i$ : photosynthetic  $\text{CO}_2$  assimilation rate ( $\mu\text{mol CO}_2 \text{m}^{-2} \text{s}^{-1}$ );  $F_s$ : steady-state fluorescence;  $F_m'$ : maximum fluorescence;  $\Delta F/F_m'$ : fluorescence yield;  $ETR$ : electron transport rate ( $\mu\text{mol m}^{-2} \text{s}^{-1}$ );  $qP$ : photochemical;  $NPQ$ : non-photochemical quenching; RMSE is pooled root mean square error from ANOVA. Different letters in the column indicate significant differences among treatments according to Tukey's test ( $p < 0.05$ ). \*  $p < 0.05$ , \*\*  $p < 0.01$ , \*\*\*  $p < 0.001$ ; ns., not significant.

18 June 2014	$G_s$	$A_i$	$F_s$	$F_m'$	$\Delta F/F_m'$	$ETR$	$qP$	$NPQ$
FIR ( $n = 12$ )	0.37	20.3	811	1221	0.33	145	0.64	5.19
INT ( $n = 12$ )	0.31	19.7	800	1183	0.32	140	0.62	5.53
NIR ( $n = 8$ )	0.39	20.1	784	1211	0.35	153	0.67	5.18
RMSE	0.08	3.38	84	145	0.04	17	0.04	0.90
Significance level	ns.	ns.	ns.	ns.	ns.	ns.	ns.	ns.
19 August 2014	$G_s$	$A_i$	$F_s$	$F_m'$	$\Delta F/F_m'$	$ETR$	$qP$	$NPQ$
FIR ( $n = 12$ )	0.17a	21.1a	827a	1213a	0.32a	139a	0.63	5.00a
INT ( $n = 12$ )	0.06b	16.0b	768b	1067b	0.28b	121b	0.59	5.89b
NIR ( $n = 12$ )	0.04b	15.4b	721b	983b	0.26b	115b	0.57	6.46b
RMSE	0.04	3.4	54	94	0.04	20	0.07	0.59
Significance level	***	**	***	***	*	*	ns	***
10 July 2015	$G_s$	$A_i$	$F_s$	$F_m'$	$\Delta F/F_m'$	$ETR$	$qP$	$NPQ$
FIR ( $n = 24$ )	0.30	7.88	694	962	0.27	117	0.57	1.88
INT ( $n = 24$ )	0.33	7.35	711	1006	0.28	124	0.59	1.93
NIR ( $n = 24$ )	0.33	9.45	694	967	0.27	117	0.57	1.87
RMSE	0.08	3.85	83	180	0.07	32	0.10	0.2
Significance level	ns.	ns.	ns.	ns.	ns.	ns.	ns.	ns.
21 September 2015	$G_s$	$A_i$	$F_s$	$F_m'$	$\Delta F/F_m'$	$ETR$	$qP$	$NPQ$
FIR ( $n = 24$ )	0.19	17.4	955	1359	0.29	128	0.56	2.10
INT ( $n = 24$ )	0.18	17.0	1008	1408	0.29	125	0.54	2.12
NIR ( $n = 24$ )	0.18	17.3	921	1369	0.32	140	0.61	2.13
RMSE	0.03	3.8	172	219	0.07	32	0.11	0.21
Significance level	ns.	ns.	ns.	ns.	ns.	ns.	ns.	ns.

**Table 3.** Pearson correlation coefficients ( $r$ ) between grapevine physiological parameters measured in 2014 and 2015.  $G_s$ : stomatal conductance ( $\text{mol H}_2\text{O m}^{-2} \text{s}^{-1}$ );  $A_i$ : photosynthetic  $\text{CO}_2$  assimilation rate ( $\mu\text{mol CO}_2 \text{m}^{-2} \text{s}^{-1}$ );  $F_s$ : steady-state fluorescence;  $F_m'$ : maximum fluorescence;  $\Delta F/F_m'$ : fluorescence yield;  $ETR$ : electron transport rate ( $\mu\text{mol m}^{-2} \text{s}^{-1}$ );  $qP$ : photochemical;  $NPQ$ : non-photochemical quenching; \*  $p < 0.05$ , \*\*  $p < 0.01$ , \*\*\*  $p < 0.001$ .

	$G_s$	$A_i$	$F_s$	$F_m'$	$\Delta F/F_m'$	$ETR$	$qP$	$NPQ$
18 June 2014								
$G_s$	1.00							
$A_i$	0.75 **	1.00						
$F_s$	0.05	0.21	1.00					
$F_m'$	0.27	0.37 **	0.85 **	1.00				
$\Delta F/F_m'$	0.39 *	0.34	0.05	0.56 **	1.00			
$ETR$	0.39 *	0.34	0.05	0.56 **	0.99 **	1.00		
$qP$	0.26	0.06	−0.32	0.16 *	0.85 **	0.85 **	1.00	
$NPQ$	−0.23	−0.31	−0.82 **	−0.97 **	−0.59 **	−0.59 **	−0.26	1.00
19 August 2014								
$G_s$	1.00							
$A_i$	0.82 **	1.00						
$F_s$	0.47 **	0.29	1.00					
$F_m'$	0.50 **	0.34 *	0.82 **	1.00				
$\Delta F/F_m'$	0.26	0.22	0.15	0.68 **	1.00			
$ETR$	0.14	0.22	0.15	0.69 **	0.99 **	1.00		
$qP$	0.13	0.14	−0.05	0.51 **	0.96 **	0.96 **	1.00	
$NPQ$	−0.50	−0.31	−0.81 **	−0.99 **	−0.69 **	−0.69 **	−0.53 **	1.00

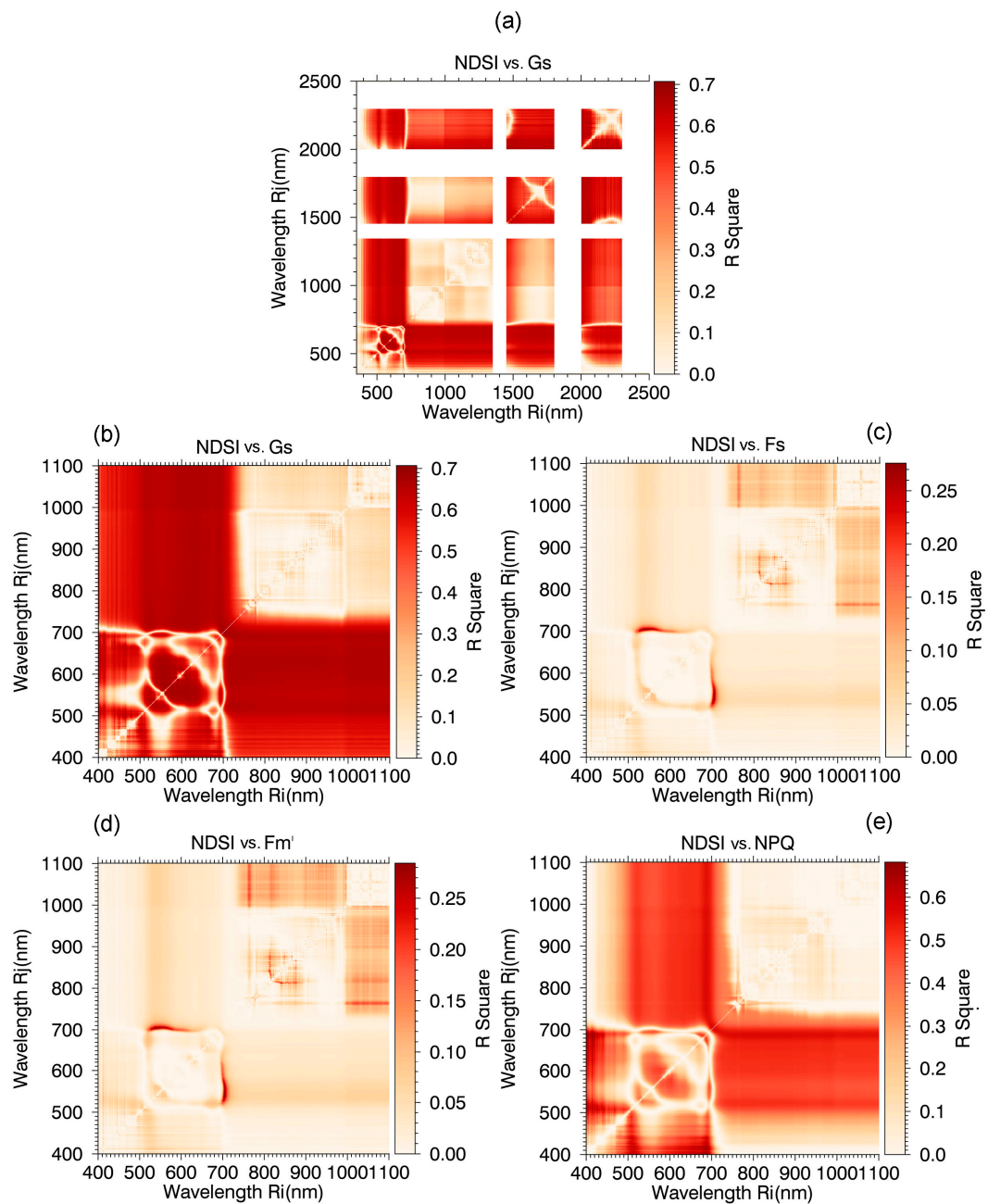


Table 3. Cont.

	$G_s$	$A_i$	$F_s$	$F_{m'}$	$\Delta F/F_{m'}$	ETR	$qP$	NPQ
<b>10 July 2015</b>								
$G_s$	1.00							
$A_i$	0.31 **	1.00						
$F_s$	−0.01	−0.08	1.00					
$F_{m'}$	−0.10	0.00	0.87 **	1.00				
$\Delta F/F_{m'}$	−0.18	−0.10	0.40 **	0.84 *	1.00			
ETR	0.19	−0.10	0.48 **	0.84 **	0.99 **	1.00		
$qP$	−0.22	−0.14	0.24 *	0.66 **	0.95 **	0.95 **	1.00	
NPQ	−0.12	−0.04	0.74 **	0.96 **	0.91 **	0.91 **	0.75 **	1.00
<b>21 September 2015</b>								
$G_s$	1.00							
$A_i$	0.76 **	1.00						
$F_s$	0.11	−0.10	1.00					
$F_{m'}$	0.29 *	0.10	0.79 **	1.00				
$\Delta F/F_{m'}$	0.26 *	0.31 **	−0.39 **	0.25 *	1.00			
ETR	0.26 *	0.31 **	−0.39 **	0.25 **	1.00 **	1.00		
$qP$	0.18	0.29 *	−0.65 **	−0.06 *	0.93 **	0.93 **	1.00	
NPQ	0.31 **	0.20	0.37 **	0.82 **	0.63 **	0.63 **	0.31 **	1.00

### 3.2. Complete-Combination Indices Analysis of the Hyperspectral Reflectance Factor Data

Figure 3a shows one of the two-dimensional maps of the coefficient of determination ( $R^2$ ) calculated using a full spectral range (350–2500 nm) and  $G_s$ . The NDSIs with the highest  $R^2$  and the lowest  $p$ -values ( $R^2 > 0.7$  and  $p < 0.001$ ) were found in the VNIR (visible and near infrared) spectral region. In most cases, the SWIR region (1300–2500 nm) correlated relatively well with  $G_s$  when only combined with the VNIR region ( $R^2 \leq 0.69$ ). The similar results were obtained for other physiological parameters, yet with very weak correlations (data not shown). The VNIR bands have a higher signal to noise ratio than SWIR bands. Besides, the SWIR bands of imaging spectroscopies tend to have lower spatial resolution than the VNIR bands due to the physical limitations. Using indices formed with the combination of VNIR and SWIR would be another source of error caused by resampling to the same spatial resolution [75]. Moreover, longer wavelengths tend to be affected by atmospheric water vapor, as the water absorption coefficient becomes higher, and it is hard to completely remove the effects of water vapor, even with a good atmospheric correction [76]. Therefore, we focused on the 400–1100 nm spectral region corresponding to VNIR bands for the rest of this study. In Table 4, the strength of the relationship between selected NDSIs and photosynthetic parameters is presented. Figure 3b–e shows a representative part of the NDSI analysis that was conducted for all leaf physiological parameters under study. The coefficient of determination ( $R^2$ ) for the relationship between the leaf reflectance factor spectra and  $G_s$  is presented in Figure 3b. The most highly correlated was NDSI( $R_{603}, R_{558}$ ) ( $R^2 = 0.720$ ;  $RMSE_{cal} = 0.063$ ) with  $G_s$  is in the yellow (570–630 nm) and green (530–580 nm) spectral region. NDSIs between the red (630–680 nm) and red-edge (690–750 nm) region also resulted in significant and high  $R^2$  ( $> 0.7$ ) values. Additionally, a broad spectral region with the combination of red and red-edge over the NIR region correlated well with  $G_s$ . In general, except NDSI( $R_{603}, R_{558}$ ) mentioned previously,  $G_s$  was also strongly correlated with other NDSIs (Table 4).



**Figure 3.** Coefficients of determination ( $R^2$ ) between grapevine physiological parameters and NDSI ( $R_i, R_j$ ) for the calibration dataset ( $n = 169$ ). (a) Stomatal conductance ( $G_s$ ) and NDSI using full spectral range (350–2500 nm); (b) stomatal conductance ( $G_s$ ) and NDSI; (c) steady-state fluorescence ( $F_s$ ) and NDSI; (d) maximum fluorescence yield ( $F_m'$ ) and NDSI; (e) non-photochemical quenching (NPQ) and NDSI.

**Table 4.** Maximum values of coefficients of determination ( $R^2$ ) and root mean square error of calibration ( $RMSE_{cal}$ ) between the grapevine physiological parameters and selected NDSIs.

Spectral Indices	$G_s$	$A_i$	$F_s$	$F_{m'}$	$NPQ$
	$R^2$ ( $RMSE_{cal}$ )	$R^2$ ( $RMSE_{cal}$ )	$R^2$ ( $RMSE_{cal}$ )	$R^2$ ( $RMSE_{cal}$ )	$R^2$ ( $RMSE_{cal}$ )
NDSI(603,558)	0.720 (0.063)	-	-	-	-
NDSI(728,525)	0.711 (0.066)	-	-	-	-
NDSI(830,525)	0.703 (0.068)	-	-	-	-
NDSI(1000,525)	0.694 (0.068)	-	-	-	-
NDSI(715,620)	0.715 (0.066)	-	-	-	-
NDSI(818,620)	0.707 (0.067)	-	-	-	-
NDSI(1000,620)	0.709 (0.067)	-	-	-	-
NDSI(726,630)	0.714 (0.068)	-	-	-	-
NDSI(778,635)	0.707 (0.069)	-	-	-	-
NDSI(1000,635)	0.707 (0.070)	-	-	-	-
NDSI(705,535)	-	0.256 (5.268)	-	-	-
NDSI(704,540)	-	-	0.275 (140.281)	-	-
NDSI(704,540)	-	-	-	0.284 (208.748)	-
NDSI(685,415)	-	-	-	-	0.681 (0.992)

Notes: The NDSIs presented here were selected according to the  $R^2$  maps, a part of which is shown in Figure 3b–e. For  $G_s$  and  $NPQ$ , NDSIs with  $R^2$  values higher than 0.7 and 0.6 are presented in this table, respectively. All relationships are significant at  $p < 0.001$  level.

The strength of the relationship between NDSIs was moderate for  $A_i$ ,  $F_s$  and  $F_{m'}$ , and negligible for  $\Delta F/F_{m'}$ ,  $ETR$  and  $qP$  (Table 4).  $A_i$  is best correlated with NDSI( $R_{705}, R_{535}$ ) ( $R^2 = 0.256$ ;  $RMSE_{cal} = 5.268$ ) and the most significant region was narrow between 520 and 550 nm. The distribution of significant spectral regions identified for the  $F_s$  and  $F_{m'}$  are very similar, as shown in Figure 3c,d. In the NDSI map (Figure 3c),  $F_s$  has a maximum  $R^2 = 0.275$  at ( $R_{704}, R_{540}$ ). This significant region was narrow (approximately 25 nm) along 700 nm ( $R_i$ ), but relatively wide over 515–595 nm ( $R_j$ ). Similarly, for  $F_{m'}$ , NDSI( $R_{704}, R_{540}$ ) with the highest  $R^2 = 0.284$  value was found in the 700–725 nm and 520–590 nm spectral regions. For both parameters, the significant spectral region extended from around 700 nm toward longer wavelengths up to 740 nm, covering the far-red chlorophyll fluorescence emission region.

The spectral region formed with blue (400–450 nm) and red (670–690 nm) regions showed the highest correlation with  $NPQ$  ( $R^2 > 0.6$ , Figure 3e). Accordingly, NDSI( $R_{681}, R_{415}$ ) within this region had a maximum  $R^2$  (0.663). NDSIs between the green (510–530 nm) and blue (400–500 nm) region also resulted in significant and high  $R^2$  values ( $>0.4$  and  $<0.6$ ). Furthermore, a broad spectral region with the combination of green and red over the NIR region showed relatively good correlation with  $NPQ$ .

Figure 4a,b shows the predictive ability of the models for the best NDSI( $R_{603}, R_{558}$ ) and NDSI( $R_{681}, R_{415}$ ) in  $G_s$  and  $NPQ$  estimation using the independent validation dataset. The significant spectral regions identified for  $G_s$  and  $NPQ$  were broad and useful in sensor applications. However, regarding the consistent and significant correlations between  $G_s$  and  $A_i$ , we only focused on  $G_s$  for the rest of the study.

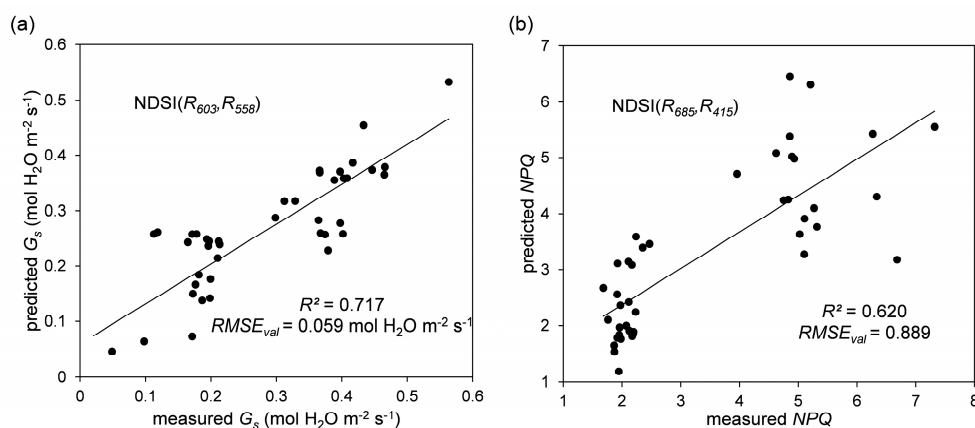


**Figure 4.** Scatter plots of predicted and measured stomatal conductance ( $G_s$ ) and non-photochemical quenching ( $NPQ$ ) values for the best NDSI models in Table 4. (a) NDSI( $R_{603}, R_{558}$ ) model and (b) NDSI( $R_{685}, R_{415}$ ) model. The  $R^2$  and  $RMSE_{val}$  are for the validation dataset ( $n = 42$ ).

### 3.3. The Relationship between the Grapevine Water Stress Response and Hyperspectral Reflectance Indices from the Literature

Table 5 summarizes the  $R^2$  and corresponding  $RMSE_{cal}$  for the previously published indices in estimation of the leaf level photosynthetic parameters.  $G_s$  showed moderate to strong correlations with mostly pigment and greenness-based indices. The best correlations were obtained with the carotenoid reflectance Index 1 (CRI1), optimized soil-adjusted vegetation index (OSAVI), NDVI and the simple ratio (SR). The modified red edge simple ratio index (mRESR) was the only index among stress based indices that was well correlated with  $G_s$ . The highest and more frequent correlations were observed for  $NPQ$  with all of the indices except for WI. The Normalized Pigment Chlorophyll Index (NPCI) appeared to be the best index for estimating the  $NPQ$  as it had the highest  $R^2$  and lowest  $RMSE_{cal}$ . Traditional indices (e.g., NDVI and SR) outperformed the improved once (EVI and triangular vegetation index (TVI)). It is worth noting that several stress based indices (e.g., PRI, plant senescence reflectance index (PSRI) and Red-Edge Vegetation Stress Index (RVSI)) showed very low to non-correlation with  $NPQ$  ( $R^2 < 0.2$ ). As opposed to  $G_s$  and  $NPQ$ , the rest of the photosynthetic parameters did not correlate well with all of the published indices ( $R^2 < 0.17$ ). Lastly, it is important to note that stress-based indices (e.g., FRI1 and FRI2), designed for chlorophyll fluorescence estimation, showed a very weak correlation with fluorescence-related photosynthetic parameters (data not shown).

**Table 5.** Coefficients of determination ( $R^2$ ) and root mean square error of calibration ( $RMSE_{cal}$ ) between the grapevine physiological parameters and indices from the literature. \*  $p < 0.05$ , \*\*  $p < 0.01$ , \*\*\*  $p < 0.001$ .

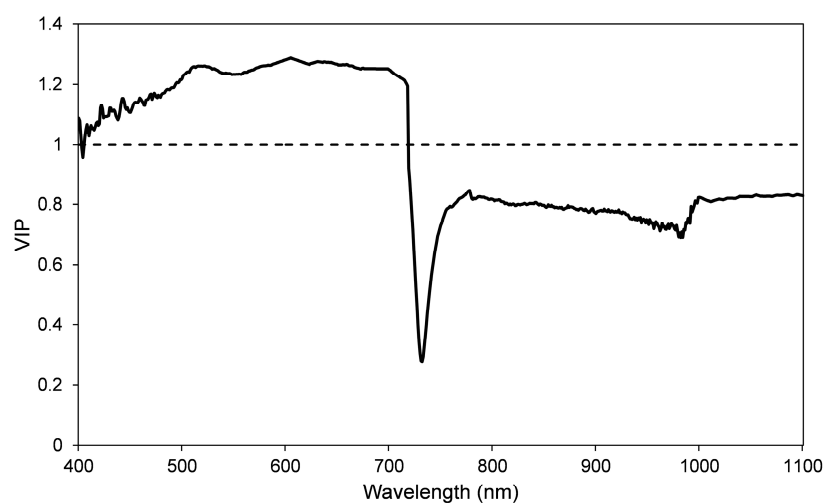
	$G_s$	$NPQ$
	$R^2$ ( $RMSE_{cal}$ )	$R^2$ ( $RMSE_{cal}$ )
<b>Leaf Pigment</b>		
Ant <sub>Gitelson</sub>	0.567 (0.100) ***	0.269 (1.509) ***
CRI1	0.663 (0.087) ***	0.332 (1.441) ***
CRI2	0.648 (0.090) ***	0.207 (1.571) ***
CI	0.648 (0.090) ***	0.529 (1.211) ***
OSAVI	0.662 (0.088) ***	0.485 (1.261) ***
RGI	0.592 (0.097) ***	0.364 (1.407) ***
SIPI	0.632 (0.092) ***	0.376 (1.394) ***
TCARI	0.537 (0.103) ***	0.368 (1.403) ***
TCARI/OSAVI	0.587 (0.098) ***	0.433 (1.327) ***
NPCI	0.518 (0.106) ***	0.544 (1.191) ***

Table 5. Cont.

	$G_s$	NPQ
	$R^2$ ( $RMSE_{cal}$ )	$R^2$ ( $RMSE_{cal}$ )
<b>Greenness</b>		
EVI	0.156 (0.140) **	0.038 (1.731) **
NDVI	0.662 (0.088) ***	0.529 (1.211) ***
GI	0.277 (0.130) ***	0.057 (1.714) **
GNDVI	0.218 (0.135) ***	0.045 (1.724) **
REIP	0.540 (0.104) ***	0.456 (1.301) ***
SR	0.680 (0.086) ***	0.531 (1.196) ***
TVI	0.257 (0.131) ***	0.086 (1.687) ***
<b>Stress</b>		
FRI <sub>1</sub>	-	0.046(1.723) **
FRI <sub>2</sub>	0.314 (0.126) ***	0.356 (1.416) ***
mRESR	0.656 (0.089) ***	0.383 (1.386) ***
NPQI	0.222 (0.134) ***	0.094 (1.680) ***
PRI	0.022 (0.151)	0.043 (1.725) **
PSRI	0.278 (0.130) ***	-
RVSI	0.263 (0.131)	-
SRPI	0.530 (0.105) ***	0.450 (1.309) ***

### 3.4. PLSR Analysis

The PLSR analysis of the hyperspectral reflectance factor data and the  $G_s$  showed that the highest  $R^2$  (0.680) and the lowest  $RMSE_{CV}$  (0.065) value were found with three factors (which explains 98.27% of the variance in the predictive variables). This PLSR model with three factors was selected based on the rule that the addition of another factor should reduce the  $RMSE_{CV}$  by more than 2% [77,78]. The influence of each wavelength in the PLSR model is illustrated in Figure 5 with corresponding VIP values. The VIP method revealed the importance of the 400–720 nm region for  $G_s$ . Particularly, the local maximum VIP values were found with 522, 604, and 700 nm, while 604 had the highest VIP value of 1.29. Figure 6 shows the predictive ability of the best PLSR model in  $G_s$  estimation using the independent validation dataset. Overall, however, the PLSR models did not result in any improvement in terms of variance explained compared to the NDSI band selection methods for  $G_s$  estimation.



**Figure 5.** Variable importance in the projection (VIP) of the partial least squares regression (PLSR) predictive model for stomatal conductance ( $G_s$ ).



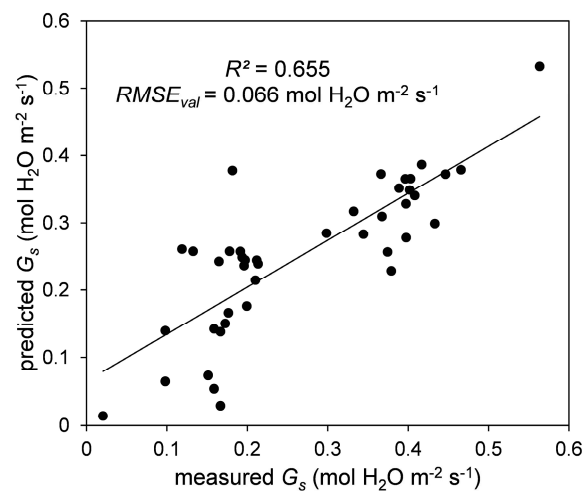


**Figure 6.** Scatter plot of predicted and measured stomatal conductance ( $G_s$ ) values for the best partial least squares regression (PLSR) predictive model. The  $R^2$  and  $RMSE_{val}$  are for the independent validation dataset ( $n = 42$ ).

### 3.5. Feasibility of Early Stress Detection

Stomatal closure induced by water stress is associated with changes in other photosynthetic parameters. Based on the significant physiological differences and absence of visible stress symptoms between treatments in August 2014, we tested the sensitivity of the best selected  $NDSI(R_{603}, R_{558})$  and the PLSR model in discriminating the difference observed in  $G_s$ . Figure 7 shows the ANOVA performed on the predicted  $G_s$  using the leaf reflectance factor data collected on 19 August 2014.  $NDSI(R_{603}, R_{557})$  (Figure 7a) was able to differentiate NIR and INT treatments from FIR treatment with a significance of  $p < 0.05$  compared to FIR treatment. The PLSR model (Figure 7b) showed similar patterns for the treatments; however, the difference is less significant ( $p > 0.05$ ) than that of Figure 7a.

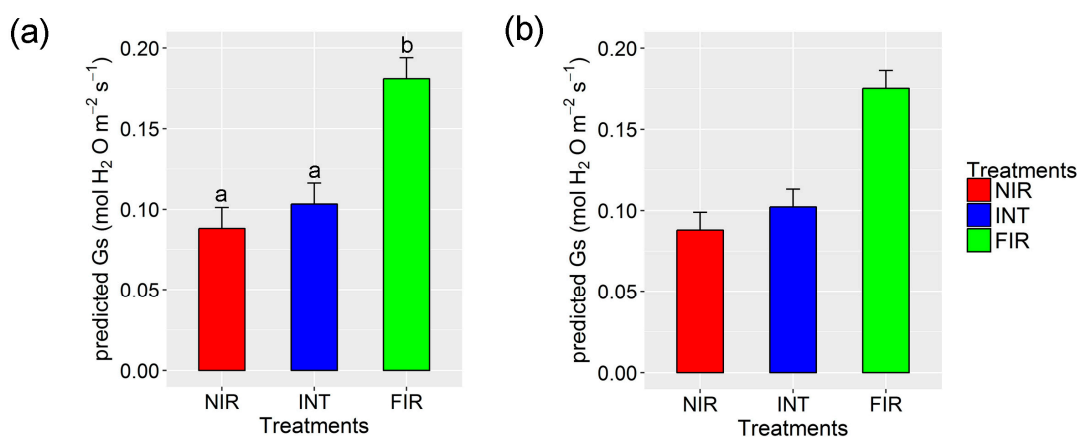


**Figure 7.** Mean values of  $NDSI(R_{601}, R_{557})$  (a) and  $rNDSI(B4, B3)$  (b) for stomatal conductance ( $G_s$ , mol  $H_2O$   $m^{-2}$   $s^{-1}$ ) measured on 19 August 2014 (DOY 231). ANOVA of each index was carried out, and different letters on the bars indicate significant differences according to the HSD Tukey's test at  $p < 0.05$ . Error bars represent pooled RMSE of the ANOVA test.

#### 4. Discussion

Pure leaf reflectance factor spectra were used in this study to assess the plant physiological response to the induced water stress using data collected on four measurement dates in 2014 and 2015.

Even though there were nine no rain days prior to the second field measurement dates in both years, the induced water stress was obvious only in 2014. This could be attributed to the drier and high temperature during the growing season of 2014 compared to 2015. After stress initiation in 2015, a partial stomatal closure was detected, but other physiological parameters were higher than before stress initiation. This could be explained by nine no rain days prior to the measurement date and lower temperature on that specific measurement date. Furthermore, the reason for this could be optimized  $G_s$  by the plants to maximize photosynthesis and minimize water loss [79].

Reduction in photosynthesis is a commonly-observed response of plants to water stress [80]. Depending on the intensity of water stress, both stomatal and non-stomatal limitations are responsible for photosynthetic decline [81,82]. The consistent and significantly positive relationship between  $G_s$  and  $A_i$  indicates that a main limiting factor for after treatment initiation could be stomatal closure. However, in a study by Zarco-Tejada et al. [83], 2013, the best relationship for  $A_i$  was found with  $F_s$  consistently for two years. This is because when grapevines are exposed to mild to moderate water stress, stomatal closure acts as a dominate photosynthetic limiting factor until  $G_s$  reaches below  $0.1 \text{ mol H}_2\text{O m}^{-2} \text{ s}^{-1}$ , if a further decrease occurs in  $G_s$  due to prolonged stress leading to noticeable change in  $F_s$  as the non-stomatal factor becomes dominant [84].

Despite the fact that there was no significant difference between treatments in most of the instances,  $G_s$  was still found to be the plant physiological parameter that showed the highest correlation with NDSIs calculated using leaf reflectance factor spectra (the highest  $R^2 = 0.720$ ). This result is in agreement with the findings of Sellers et al. [85], Myneni et al. [86], Verma et al. [87] and Carter [88], who reported strong linear or non-linear relationships between vegetation indices calculated using VIS and NIR bands, and  $G_s$ .  $G_s$  is an integrative stress indicator by responding to all external (soil water availability and vapor pressure deficit) and internal (abscisic acid, xylem conductivity, chlorophyll content and leaf water status) influences caused by water stress [89–92]. This may explain the broad spectral regions with the combination of different wavelengths that correlated well with  $G_s$ .  $\text{NDSI}(R_{728}, R_{525})$ ,  $\text{NDSI}(R_{715}, R_{620})$  and  $\text{NDSI}(R_{726}, R_{630})$  for  $G_s$  and  $\text{NDSI}(R_{705}, R_{535})$  for  $A_i$  emphasized the importance the red-edge region (695–730 nm). These results agree with the findings of Carter [88], who reported that the red-edge region around 701 nm is the most suitable for  $G_s$  and  $A_i$  estimation because of its sensitivity to subtle changes in chlorophyll. Evidently, the red-edge region is sensitive to chlorophyll concentration, but this region is also sensitive to changes in cell structure as it is closer to the NIR region. Therefore, the red-edge region is more likely to respond to changes in leaf cell structure separate from pigmentation [93,94]. This could explain why  $\text{NDSI}(603, 558)$  was superior, where green and yellow bands are less sensitive to changes in leaf structure and water content [95]. Furthermore, both green and yellow bands are known to be sensitive to subtle changes in photosynthetic pigments [58,95,96]. In addition, the yellow band highlights the negative change in slope from the green peak around 550 nm [97]. Figure 8 depicts the effects of irrigation treatments on leaf reflectance factor spectra. Apparently, the effect of treatments on 557 nm is minimum, whereas 603 nm is highly effected by treatments. It is also worth noting that 603 nm is separate from the strong chlorophyll absorption band 680 nm, which is less sensitive to more subtle changes in photosynthesis pigment concentrations [98,99].

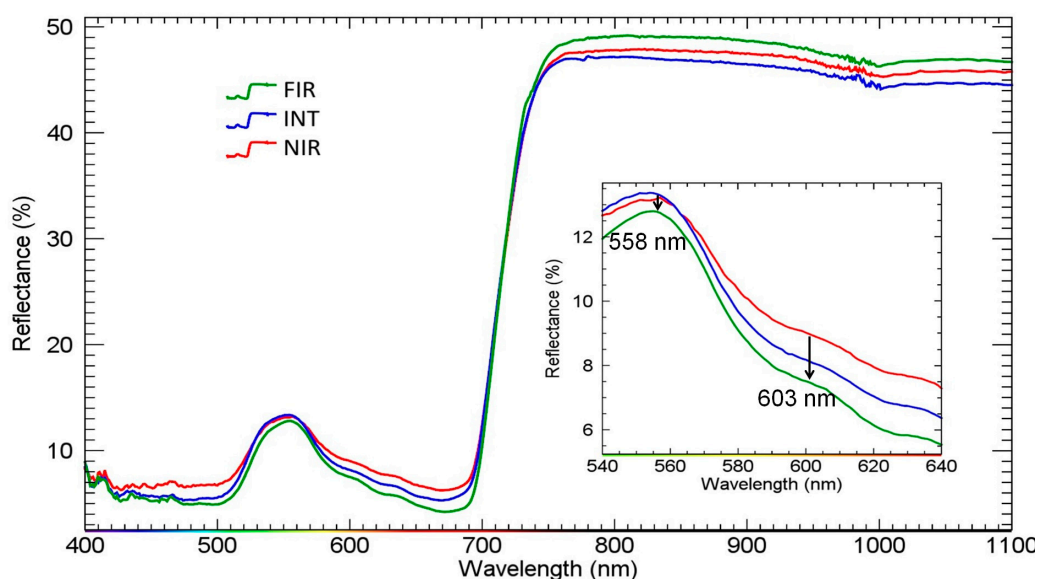


**Figure 8.** Mean reflectance factor spectra collected on 19 August 2014 for the different irrigation treatments.

A very similar and significant combination of spectral regions ( $R^2$  is highest at 704 and 540 nm) was found for  $F_s$  and  $F_m'$ , and these results somewhat agree with the findings of Stratoulas et al. [40], who reported the combination of similar spectral regions (including red and far-red fluorescence emission regions) correlated with  $F_s$  and  $F_m'$  for deep water reed plants with lower chlorophyll concentration, but the shapes of the  $R^2$  maps from their study showed broad significant spectral regions with diffuse edges compared to the ones in our study (Figure 4b,c). Although plants only emit 2–5% of the absorbed sun light energy as fluorescence, the fluorescence emission spectrum spans a broad spectral region of red and far-red (600–800 nm) with two distinct peaks at around 685–690 nm and 730–740 nm [100,101]. The red part of the fluorescence emission is subject to reabsorption because this part of the fluorescence emission spectrum overlaps with the chlorophyll absorption spectrum, while the far-red part is minimally affected [102,103]. Therefore, red fluorescence emission is low at the sensor especially when chlorophyll is not markedly damaged, and this explains why our identified significant spectral regions were located in far-red region for both  $F_s$  and  $F_m'$ .

NDSIs calculated with leaf reflectance factor spectra were weakly correlated with  $\Delta F/F_m'$ ,  $ETR$  and  $qP$ . This could be explained by the high level heterogeneity of grapevines photosynthetic activity affected by irrigation treatments, even though the differences in grapevine physiology were not consistently significant. In contrast, there was a strong correlation between NDSIs and  $NPQ$ , and the strength of the correlation was comparable to that of  $G_s$ , suggesting that grapevines were more subject to photosynthetic down-regulation via  $NPQ$ , probably related to the xanthophyll cycle [104,105]. In general,  $NDSI(R_{685}, R_{415})$  showed the highest correlation for  $NPQ$  and selected spectral bands corresponding to the absorption maxima of chlorophyll and carotenoids. The latter compose the xanthophyll cycle to protect the PSII from photodamage by thermal dissipation [104].

$G_s$  response to a subtle leaf internal structure and pigment changes could explain the moderate to low (yet frequent) correlation of greenness and pigment-based indices from the literature with  $G_s$ . The NDSIs identified for  $G_s$  showed  $R^2$  higher than 0.7, while the best performed indices from the literature had the highest  $R^2$  of 0.68. These results are somewhat expected regarding RGI and NDVI because these indices were the specific cases of NDSIs, and their correlations with  $G_s$  were already accounted for. Similarly, for  $NPQ$ , the NPCI band combination of  $(R_{680}, R_{430})$  showed the highest  $R^2$  among the indices from the literature, while the best identified  $NDSI(R_{685}, R_{415})$  had the  $R^2$  of 0.681. Moreover, the spectral bands used for these indices can be found within the same spectral regions, e.g., red and blue regions, and therefore, similar outputs are expected. The PRI, an indicator

of the epoxidation state of xanthophyll, turns out to be one of the worst performing indices. This is because PRI captures short-term plant photosynthetic performance in response to environmental conditions; for the long term; however, variation in plant structure and foliar pigment concentration act as confounding factors for elucidating the temporal photosynthetic status by using PRI [106–110].

Compared with the NDSI method, the PLSR method did not improve the predictive ability of the model. However, VIP values indicated the importance of the yellow wavelength region. This is consistent to some extent with a recent study conducted by Zengeya et al. [97], who found that the WorldVidw-2 yellow band improved the detection of low nitrogen level within savanna grasses especially at the beginning of the dry season, while the red-edge band was weakly correlated with low nitrogen levels. Up to 75% of the leaf nitrogen is in the chloroplasts that contains chlorophyll [111], and the sensitivity of the yellow band to a low level of nitrogen could be attributed to subtle changes in chlorophyll concentration at the beginning of the dry season, thus  $G_s$ . Additionally, Inoue et al. [112] reported the inferior performance of the multivariate models compared to index-based models in canopy chlorophyll content estimation.

Field-measured physiological data in our study presented a relatively wide range of stress by showing significant physiological differences between treatments, and this was especially true for the data collected on the second measurement date (DOY 231) in 2014. Such a difference allowed us to test the capability of effective  $NDSI(R_{603}, R_{558})$  in early stress detection.

The two-dimensional maps of  $R^2$  provide a clear overview of effective wavebands and spectral regions for determining optimal normalized indices to predict various parameters under study [35]. Alternatively, multivariate regression methods, machine learning-based support vector machine and non-linear machine learning methods can be employed for leveraging spectral data [15,113,114]. However, these methods are dependent on a large number of high quality training datasets, and their operational applicability is limited [113,115,116].

## 5. Conclusions

The objectives of this contribution were to (1) investigate the potential of field spectroscopy for characterizing the physiological status of grapevines exposed to different levels of water stress based on in situ measurements and (2) identify the most effective indices and predictive models to evaluate the potential of visible and near-infrared band combinations in the early detection of plant response to water stress. To this end, we utilized leaf reflectance factor spectra and plant physiological parameters measured in a vineyard treated with three different irrigation treatments throughout two consecutive growing seasons. Consistently significant correlation in both experimental years was only found between in situ measured leaf level  $A_i$  and  $G_s$ , suggesting that stomatal closure acted as a dominate photosynthetic limiting factor. Strong correlations between leaf reflectance factor spectra and plant physiological status demonstrated the potential of ground-based spectroscopy in determining plant photosynthetic performance regardless of different irrigation treatments, growth stages and other environmental factors. In particular, we found that  $NDSI(R_{603}, R_{558})$  showed the highest  $R^2$  (0.720) for  $G_s$  and  $NDSI(R_{685}, R_{415})$  for  $NPQ$  ( $R^2 = 0.681$ ). These indices are spectrally wide and applicable for broad satellite bands. The PLSR model performance was inferior to the NDSI-based method. However, the VIP method provided insights into the importance of the yellow region, confirming that the yellow band improves the prediction ability of hyperspectral reflectance factor data in  $G_s$  within the vineyard. Nevertheless, this study only relied on ground-based field spectroscopy. Therefore, the applicability of our findings as an operational tool for predicting plant early stress indicators requires validation using the air- and space-borne data acquired over different plant species exposed to water stress. Scaling up these findings to satellite observations by canopy radiative transfer simulations, unmanned aerial systems-based imaging and current and future satellites systems is the future work of this research.

**Acknowledgments:** Funding for this work was provided by National Science Foundation (IIA-1355406 and IIA-1430427), NASA (NNX15AK03H), the Grape and Wine Institute at the University of Missouri and the Center for Sustainability at Saint Louis University. The authors thank Maitiniyazi Maimaitijiang, Sean Hartling, Mark Grzovic, Bethany Marshall, Guzhalaiyi Sataer and Arafat Kahar who assisted long and strenuous hours to collect field data. The authors also thank the editor and the anonymous reviewers for their thoughtful review and constructive comments.

**Author Contributions:** Abduwasit Ghulam, Misha T. Kwasniewski and Arianna Bozzolo conceived of and designed the experiments. Matthew Maimaitiyiming, Arianna Bozzolo and Joseph L. Wilkins performed the experiments. Matthew Maimaitiyiming analyzed the data and wrote the paper.

**Conflicts of Interest:** The authors declare no conflict of interest.

## References

1. Turral, H.; Burke, J.; Faurès, J.M. *Climate Change, Water and Food Security*; Food and Agriculture Organization of the United Nations (FAO): Rome, Italy, 2011.
2. Hsiao, T.; Fereres, E.; Acevedo, E.; Henderson, D. Water stress and dynamics of growth and yield of crop plants. In *Water and Plant Life*; Springer: Berlin, Germany, 1976; pp. 281–305.
3. Vivier, M.A.; Pretorius, I.S. Genetically tailored grapevines for the wine industry. *Trends Biotechnol.* **2002**, *20*, 472–478. [[CrossRef](#)]
4. Stonebridge Research Group. *The Economic Impact of Wine and Grape in Missouri*; Stonebridge Research Group™ LLC: St.Helena, CA, USA, 2010; p. 26.
5. Dai, A. Drought under global warming: A review. *Wiley Interdiscip. Rev. Clim. Chang.* **2011**, *2*, 45–65. [[CrossRef](#)]
6. Chaves, M. Effects of water deficits on carbon assimilation. *J. Exp. Bot.* **1991**, *42*, 1–16. [[CrossRef](#)]
7. Jackson, R.D.; Idso, S.; Reginato, R.; Pinter, P. Canopy temperature as a crop water stress indicator. *Water Resour. Res.* **1981**, *17*, 1133–1138. [[CrossRef](#)]
8. Krause, G.H. Photoinhibition of photosynthesis. An evaluation of damaging and protective mechanisms. *Physiol. Plant.* **1988**, *74*, 566–574. [[CrossRef](#)]
9. Baker, N.R.; Rosenqvist, E. Applications of chlorophyll fluorescence can improve crop production strategies: An examination of future possibilities. *J. Exp. Bot.* **2004**, *55*, 1607–1621. [[CrossRef](#)] [[PubMed](#)]
10. Lisar, S.Y.; Motafakkerazad, R.; Hossain, M.M.; Rahman, I.M. *Water Stress in Plants: Causes, Effects and Responses*; InTech: Rijeka, Croatia, 2012.
11. Lim, P.; Nam, H. Aging and senescence of the leaf organ. *J. Plant Biol.* **2007**, *50*, 291–300. [[CrossRef](#)]
12. Lichtenthaler, H.K. The stress concept in plants: An introduction. *Ann. N. Y. Acad. Sci.* **1998**, *851*, 187–198. [[CrossRef](#)] [[PubMed](#)]
13. Bouman, B.; Van Keulen, H.; Van Laar, H.; Rabbinge, R. The ‘school of de wit’ crop growth simulation models: A pedigree and historical overview. *Agric. Syst.* **1996**, *52*, 171–198. [[CrossRef](#)]
14. Thenkabail, A.; Lyon, P.S.; Huete, J.G. *Hyperspectral Remote Sensing of Vegetation*; CRC Press: Boca Raton, FL, USA, 2011.
15. Clevers, J.G.; Kooistra, L.; Schaepman, M.E. Estimating canopy water content using hyperspectral remote sensing data. *Int. J. Appl. Earth Obs. Geoinform.* **2010**, *12*, 119–125. [[CrossRef](#)]
16. Viña, A.; Gitelson, A.A. Sensitivity to foliar anthocyanin content of vegetation indices using green reflectance. *IEEE Geosci. Remote Sens.* **2011**, *8*, 464–468. [[CrossRef](#)]
17. Jensen, J.R. *Remote Sensing of the Environment: An Earth Resource Perspective 2/e*; Pearson Prentice Hall: Upper Saddle River, NJ, USA, 2007.
18. Elvidge, C.D. Visible and near infrared reflectance characteristics of dry plant materials. *Int. J. Remote Sens.* **1990**, *11*, 1775–1795. [[CrossRef](#)]
19. Tucker, C.J. Red and photographic infrared linear combinations for monitoring vegetation. *Remote Sens. Environ.* **1979**, *8*, 127–150. [[CrossRef](#)]
20. Sims, D.A.; Gamon, J.A. Relationships between leaf pigment content and spectral reflectance across a wide range of species, leaf structures and developmental stages. *Remote Sens. Environ.* **2002**, *81*, 337–354. [[CrossRef](#)]
21. Thenkabail, P.S.; Smith, R.B.; De Pauw, E. Hyperspectral vegetation indices and their relationships with agricultural crop characteristics. *Remote Sens. Environ.* **2000**, *71*, 158–182. [[CrossRef](#)]



22. Thenkabail, P.S.; Teluguntla, P.G.; Gumma, M.K.; Dheeravath, V. *Hyperspectral Remote Sensing for Terrestrial Applications. Land Resources Monitoring, Modeling, and Mapping With Remote Sensing*; CRC Press: Boca Raton, FL, USA, 2015; pp. 201–233.
23. Panigada, C.; Rossini, M.; Meroni, M.; Cilia, C.; Busetto, L.; Amaducci, S.; Boschetti, M.; Cogliati, S.; Picchi, V.; Pinto, F. Fluorescence, pri and canopy temperature for water stress detection in cereal crops. *Int. J. Appl. Earth Obs. Geoinform.* **2014**, *30*, 167–178. [[CrossRef](#)]
24. Gamon, J.; Penuelas, J.; Field, C. A narrow-waveband spectral index that tracks diurnal changes in photosynthetic efficiency. *Remote Sens. Environ.* **1992**, *41*, 35–44. [[CrossRef](#)]
25. Suárez, L.; Zarco-Tejada, P.J.; Berni, J.A.; González-Dugo, V.; Fereres, E. Modelling pri for water stress detection using radiative transfer models. *Remote Sens. Environ.* **2009**, *113*, 730–744. [[CrossRef](#)]
26. Krause, G.H.; Weis, E. Chlorophyll fluorescence as a tool in plant physiology. *Photosynth. Res.* **1984**, *5*, 139–157. [[CrossRef](#)] [[PubMed](#)]
27. Guanter, L.; Rossini, M.; Colombo, R.; Meroni, M.; Frankenberg, C.; Lee, J.-E.; Joiner, J. Using field spectroscopy to assess the potential of statistical approaches for the retrieval of sun-induced chlorophyll fluorescence from ground and space. *Remote Sens. Environ.* **2013**, *133*, 52–61. [[CrossRef](#)]
28. Guanter, L.; Zhang, Y.; Jung, M.; Joiner, J.; Voigt, M.; Berry, J.A.; Frankenberg, C.; Huete, A.R.; Zarco-Tejada, P.; Lee, J.-E. Global and time-resolved monitoring of crop photosynthesis with chlorophyll fluorescence. *Proc. Natl. Acad. Sci. USA* **2014**, *111*, E1327–E1333. [[CrossRef](#)] [[PubMed](#)]
29. Moya, I.; Camenen, L.; Evain, S.; Goulas, Y.; Cerovic, Z.G.; Latouche, G.; Flexas, J.; Ounis, A. A new instrument for passive remote sensing: 1. Measurements of sunlight-induced chlorophyll fluorescence. *Remote Sens. Environ.* **2004**, *91*, 186–197. [[CrossRef](#)]
30. Meroni, M.; Rossini, M.; Guanter, L.; Alonso, L.; Rascher, U.; Colombo, R.; Moreno, J. Remote sensing of solar-induced chlorophyll fluorescence: Review of methods and applications. *Remote Sens. Environ.* **2009**, *113*, 2037–2051. [[CrossRef](#)]
31. Zarco-Tejada, P.J.; Berni, J.A.; Suárez, L.; Sepulcre-Cantó, G.; Morales, F.; Miller, J.R. Imaging chlorophyll fluorescence with an airborne narrow-band multispectral camera for vegetation stress detection. *Remote Sens. Environ.* **2009**, *113*, 1262–1275. [[CrossRef](#)]
32. Zarco-Tejada, P.J.; González-Dugo, V.; Berni, J.A. Fluorescence, temperature and narrow-band indices acquired from a uav platform for water stress detection using a micro-hyperspectral imager and a thermal camera. *Remote Sens. Environ.* **2012**, *117*, 322–337. [[CrossRef](#)]
33. Ashourloo, D.; Mobasheri, M.R.; Huete, A. Developing two spectral disease indices for detection of wheat leaf rust (puccinia triticina). *Remote Sens.* **2014**, *6*, 4723–4740. [[CrossRef](#)]
34. Delalieux, S.; Auwerkerken, A.; Verstraeten, W.W.; Somers, B.; Valcke, R.; Lhermitte, S.; Keulemans, J.; Coppin, P. Hyperspectral reflectance and fluorescence imaging to detect scab induced stress in apple leaves. *Remote Sens.* **2009**, *1*, 858–874. [[CrossRef](#)]
35. Inoue, Y.; Peñuelas, J.; Miyata, A.; Mano, M. Normalized difference spectral indices for estimating photosynthetic efficiency and capacity at a canopy scale derived from hyperspectral and co<sub>2</sub> flux measurements in rice. *Remote Sens. Environ.* **2008**, *112*, 156–172. [[CrossRef](#)]
36. Inoue, Y.; Sakaiya, E.; Zhu, Y.; Takahashi, W. Diagnostic mapping of canopy nitrogen content in rice based on hyperspectral measurements. *Remote Sens. Environ.* **2012**, *126*, 210–221. [[CrossRef](#)]
37. Marshall, M.; Thenkabail, P.; Biggs, T.; Post, K. Hyperspectral narrowband and multispectral broadband indices for remote sensing of crop evapotranspiration and its components (transpiration and soil evaporation). *Agric. For. Meteorol.* **2016**, *218*, 122–134. [[CrossRef](#)]
38. Pôças, I.; Rodrigues, A.; Gonçalves, S.; Costa, P.M.; Gonçalves, I.; Pereira, L.S.; Cunha, M. Predicting grapevine water status based on hyperspectral reflectance vegetation indices. *Remote Sens.* **2015**, *7*, 16460–16479. [[CrossRef](#)]
39. Stagakis, S.; Markos, N.; Sykioti, O.; Kyparissis, A. Monitoring canopy biophysical and biochemical parameters in ecosystem scale using satellite hyperspectral imagery: An application on a phlomis fruticosa mediterranean ecosystem using multiangular chris/proba observations. *Remote Sens. Environ.* **2010**, *114*, 977–994. [[CrossRef](#)]
40. Stratoulis, D.; Balzter, H.; Zlinszky, A.; Tóth, V.R. Assessment of ecophysiology of lake shore reed vegetation based on chlorophyll fluorescence, field spectroscopy and hyperspectral airborne imagery. *Remote Sens. Environ.* **2015**, *157*, 72–84. [[CrossRef](#)]

41. Asner, G.P.; Martin, R.E.; Anderson, C.B.; Knapp, D.E. Quantifying forest canopy traits: Imaging spectroscopy versus field survey. *Remote Sens. Environ.* **2015**, *158*, 15–27. [[CrossRef](#)]
42. Sawut, M.; Ghulam, A.; Tiyyip, T.; Zhang, Y.-J.; Ding, J.-L.; Zhang, F.; Maimaitiyiming, M. Estimating soil sand content using thermal infrared spectra in arid lands. *Int. J. Appl. Earth Obs. Geoinform.* **2014**, *33*, 203–210. [[CrossRef](#)]
43. Boulesteix, A.-L.; Strimmer, K. Partial least squares: A versatile tool for the analysis of high-dimensional genomic data. *Brief. Bioinform.* **2006**, *8*, 32–44. [[CrossRef](#)] [[PubMed](#)]
44. Martens, H.; Martens, M. Analysis of two data tables x and y: Partial least squares regression (pls). In *Multivariate Analysis of Quality: An Introduction*; Wiley: London, UK, 2001; pp. 111–125.
45. Feilhauer, H.; Asner, G.P.; Martin, R.E. Multi-method ensemble selection of spectral bands related to leaf biochemistry. *Remote Sens. Environ.* **2015**, *164*, 57–65. [[CrossRef](#)]
46. Genty, B.; Briantais, J.-M.; Baker, N.R. The relationship between the quantum yield of photosynthetic electron transport and quenching of chlorophyll fluorescence. *Biochim. Biophys. Acta (BBA)-Gen. Subj.* **1989**, *990*, 87–92. [[CrossRef](#)]
47. Schaepman-Strub, G.; Schaepman, M.; Painter, T.; Dangel, S.; Martonchik, J. Reflectance quantities in optical remote sensing—definitions and case studies. *Remote Sens. Environ.* **2006**, *103*, 27–42. [[CrossRef](#)]
48. Gitelson, A.A.; Gritz, Y.; Merzlyak, M.N. Relationships between leaf chlorophyll content and spectral reflectance and algorithms for non-destructive chlorophyll assessment in higher plant leaves. *J. Plant Physiol.* **2003**, *160*, 271–282. [[CrossRef](#)] [[PubMed](#)]
49. Gitelson, A.A.; Zur, Y.; Chivkunova, O.B.; Merzlyak, M.N. Assessing carotenoid content in plant leaves with reflectance spectroscopy. *Photochem. Photobiol.* **2002**, *75*, 272–281. [[CrossRef](#)]
50. Gitelson, A.; Merzlyak, M.N. Quantitative estimation of chlorophyll-a using reflectance spectra: Experiments with autumn chestnut and maple leaves. *J. Photochem. Photobiol. B Biol.* **1994**, *22*, 247–252. [[CrossRef](#)]
51. Rondeaux, G.; Steven, M.; Baret, F. Optimization of soil-adjusted vegetation indices. *Remote Sens. Environ.* **1996**, *55*, 95–107. [[CrossRef](#)]
52. Zarco-Tejada, P.J.; Berjón, A.; López-Lozano, R.; Miller, J.R.; Martín, P.; Cachorro, V.; González, M.; De Frutos, A. Assessing vineyard condition with hyperspectral indices: Leaf and canopy reflectance simulation in a row-structured discontinuous canopy. *Remote Sens. Environ.* **2005**, *99*, 271–287. [[CrossRef](#)]
53. Penuelas, J.; Frederic, B.; Filella, I. Semi-empirical indices to assess carotenoids/chlorophyll a ratio from leaf spectral reflectance. *Photosynthetica* **1995**, *31*, 221–230.
54. Haboudane, D.; Miller, J.R.; Tremblay, N.; Zarco-Tejada, P.J.; Dextraze, L. Integrated narrow-band vegetation indices for prediction of crop chlorophyll content for application to precision agriculture. *Remote Sens. Environ.* **2002**, *81*, 416–426. [[CrossRef](#)]
55. Peñuelas, J.; Gamon, J.; Fredeen, A.; Merino, J.; Field, C. Reflectance indices associated with physiological changes in nitrogen-and water-limited sunflower leaves. *Remote Sens. Environ.* **1994**, *48*, 135–146. [[CrossRef](#)]
56. Huete, A.; Didan, K.; Miura, T.; Rodriguez, E.P.; Gao, X.; Ferreira, L.G. Overview of the radiometric and biophysical performance of the modis vegetation indices. *Remote Sens. Environ.* **2002**, *83*, 195–213. [[CrossRef](#)]
57. Rouse, J.W., Jr.; Haas, R.; Schell, J.; Deering, D. Monitoring Vegetation Systems in the Great Plains with ERTS. In *Proceedings of the Third Earth Resources Technology Satellite-1 Symposium*, Washington, DC, USA, 10–14 December 1973.
58. Gitelson, A.A.; Kaufman, Y.J.; Merzlyak, M.N. Use of a green channel in remote sensing of global vegetation from eos-modis. *Remote Sens. Environ.* **1996**, *58*, 289–298. [[CrossRef](#)]
59. Guyot, G.; Baret, F.; Major, D. High spectral resolution: Determination of spectral shifts between the red and the near infrared. *Int. Arch. Photogramm. Remote Sens.* **1988**, *11*, 750–760.
60. Haboudane, D.; Miller, J.R.; Pattey, E.; Zarco-Tejada, P.J.; Strachan, I.B. Hyperspectral vegetation indices and novel algorithms for predicting green lai of crop canopies: Modeling and validation in the context of precision agriculture. *Remote Sens. Environ.* **2004**, *90*, 337–352. [[CrossRef](#)]
61. Dobrowski, S.; Pushnik, J.; Zarco-Tejada, P.J.; Ustin, S. Simple reflectance indices track heat and water stress-induced changes in steady-state chlorophyll fluorescence at the canopy scale. *Remote Sens. Environ.* **2005**, *97*, 403–414. [[CrossRef](#)]
62. Barnes, J.; Balaguer, L.; Manrique, E.; Elvira, S.; Davison, A. A reappraisal of the use of dmso for the extraction and determination of chlorophylls a and b in lichens and higher plants. *Environ. Exp. Bot.* **1992**, *32*, 85–100. [[CrossRef](#)]

63. Merzlyak, M.N.; Gitelson, A.A.; Chivkunova, O.B.; Rakitin, V.Y. Non-destructive optical detection of pigment changes during leaf senescence and fruit ripening. *Physiol. Plant.* **1999**, *106*, 135–141. [[CrossRef](#)]
64. Merton, R.; Huntington, J. In early simulation results of the aries-1 satellite sensor for multi-temporal vegetation research derived from aviris. In Proceedings of the Eighth Annual JPL Airborne Earth Science Workshop, Pasadena, CA, USA, 9–11 February 1999; pp. 8–14.
65. Penˆ Uelas, J.; Filella, I.; Lloret, P.; Munˆ OZ, F.; Vilajeliu, M. Reflectance assessment of mite effects on apple trees. *Int. J. Remote Sens.* **1995**, *16*, 2727–2733. [[CrossRef](#)]
66. Pe˜uelas, J.; Filella, I.; Biel, C.; Serrano, L.; Save, R. The reflectance at the 950–970 nm region as an indicator of plant water status. *Int. J. Remote Sens.* **1993**, *14*, 1887–1905. [[CrossRef](#)]
67. Haaland, D.M.; Thomas, E.V. Partial least-squares methods for spectral analyses. 1. Relation to other quantitative calibration methods and the extraction of qualitative information. *Anal. Chem.* **1988**, *60*, 1193–1202. [[CrossRef](#)]
68. Geladi, P.; Kowalski, B.R. Partial least-squares regression: A tutorial. *Anal. Chim. Acta* **1986**, *185*, 1–17. [[CrossRef](#)]
69. Martens, H.; Naes, T. *Multivariate Calibration*; John Wiley & Sons: Hoboken, NJ, USA, 1992.
70. Wold, S.; Sjöström, M.; Eriksson, L. PLS-regression: A basic tool of chemometrics. *Chemom. Intell. Lab. Syst.* **2001**, *58*, 109–130. [[CrossRef](#)]
71. Eriksson, L. *Introduction to Multi-and Megavariate Data Analysis Using Projection Methods (Pca & Pls)*; Umetrics AB: Malmö, Sweden, 1999.
72. Flexas, J.; Bota, J.; Escalona, J.M.; Sampol, B.; Medrano, H. Effects of drought on photosynthesis in grapevines under field conditions: An evaluation of stomatal and mesophyll limitations. *Funct. Plant Biol.* **2002**, *29*, 461–471. [[CrossRef](#)]
73. Gollan, T.; Turner, N.; Schulze, E.-D. The responses of stomata and leaf gas exchange to vapour pressure deficits and soil water content. *Oecologia* **1985**, *65*, 356–362. [[CrossRef](#)] [[PubMed](#)]
74. Socias, X.; Correia, M.; Chaves, M.; Medrano, H. The role of abscisic acid and water relations in drought responses of subterranean clover. *J. Exp. Bot.* **1997**, *48*, 1281–1288. [[CrossRef](#)]
75. Hunt, E.R., Jr.; Daughtry, C.S.; Li, L. Feasibility of estimating leaf water content using spectral indices from worldview-3's near-infrared and shortwave infrared bands. *Int. J. Remote Sens.* **2016**, *37*, 388–402. [[CrossRef](#)]
76. Ghulam, A.; Li, Z.-L.; Qin, Q.; Tong, Q.; Wang, J.; Kasimu, A.; Zhu, L. A method for canopy water content estimation for highly vegetated surfaces-shortwave infrared perpendicular water stress index. *Sci. China Ser. D Earth Sci.* **2007**, *50*, 1359–1368. [[CrossRef](#)]
77. Chen, J.; Gu, S.; Shen, M.; Tang, Y.; Matsushita, B. Estimating aboveground biomass of grassland having a high canopy cover: An exploratory analysis of in situ hyperspectral data. *Int. J. Remote Sens.* **2009**, *30*, 6497–6517. [[CrossRef](#)]
78. Cho, M.A.; Skidmore, A.; Corsi, F.; Van Wieren, S.E.; Sobhan, I. Estimation of green grass/herb biomass from airborne hyperspectral imagery using spectral indices and partial least squares regression. *Int. J. Appl. Earth Obs. Geoinform.* **2007**, *9*, 414–424. [[CrossRef](#)]
79. Cowan, I.; Farquhar, G. Stomatal Functioning in Relation to Leaf Metabolism and Environment. In *Integration of Activity in the Higher Plant*; Cambridge University Press: Cambridge, UK, 1977; pp. 471–505.
80. Anjum, S.A.; Xie, X.-Y.; Wang, L.-C.; Saleem, M.F.; Man, C.; Lei, W. Morphological, physiological and biochemical responses of plants to drought stress. *Afr. J. Agric. Res.* **2011**, *6*, 2026–2032.
81. Chaves, M.M.; Maroco, J.P.; Pereira, J.S. Understanding plant responses to drought—From genes to the whole plant. *Funct. Plant Biol.* **2003**, *30*, 239–264. [[CrossRef](#)]
82. Xu, Z.; Zhou, G. Responses of leaf stomatal density to water status and its relationship with photosynthesis in a grass. *J. Exp. Bot.* **2008**, *59*, 3317–3325. [[CrossRef](#)] [[PubMed](#)]
83. Zarco-Tejada, P.J.; Ca talina, A.; González, M.; Martín, P. Relationships between net photosynthesis and steady-state chlorophyll fluorescence retrieved from airborne hyperspectral imagery. *Remote Sens. Environ.* **2013**, *136*, 247–258. [[CrossRef](#)]
84. Flexas, J.; Escalona, J.M.; Evain, S.; Gulías, J.; Moya, I.; Osmond, C.B.; Medrano, H. Steady-state chlorophyll fluorescence (fs) measurements as a tool to follow variations of net co2 assimilation and stomatal conductance during water-stress in c3 plants. *Physiol. Plant.* **2002**, *114*, 231–240. [[CrossRef](#)] [[PubMed](#)]

85. Sellers, P.; Berry, J.; Collatz, G.; Field, C.; Hall, F. Canopy reflectance, photosynthesis, and transpiration. Iii. A reanalysis using improved leaf models and a new canopy integration scheme. *Remote Sens. Environ.* **1992**, *42*, 187–216. [[CrossRef](#)]
86. Myneni, R.; Ganapol, B.; Asrar, G. Remote sensing of vegetation canopy photosynthetic and stomatal conductance efficiencies. *Remote Sens. Environ.* **1992**, *42*, 217–238. [[CrossRef](#)]
87. Verma, S.; Sellers, P.; Walthall, C.; Hall, F.; Kim, J.; Goetz, S. Photosynthesis and stomatal conductance related to reflectance on the canopy scale. *Remote Sens. Environ.* **1993**, *44*, 103–116. [[CrossRef](#)]
88. Carter, G.A. Reflectance wavebands and indices for remote estimation of photosynthesis and stomatal conductance in pine canopies. *Remote Sens. Environ.* **1998**, *63*, 61–72. [[CrossRef](#)]
89. Davies, W.J.; Zhang, J. Root signals and the regulation of growth and development of plants in drying soil. *Ann. Rev. Plant Biol.* **1991**, *42*, 55–76. [[CrossRef](#)]
90. Matsumoto, K.; Ohta, T.; Tanaka, T. Dependence of stomatal conductance on leaf chlorophyll concentration and meteorological variables. *Agric. For. Meteorol.* **2005**, *132*, 44–57. [[CrossRef](#)]
91. Medrano, H.; Escalona, J.M.; Bota, J.; Gulías, J.; Flexas, J. Regulation of photosynthesis of c3 plants in response to progressive drought: Stomatal conductance as a reference parameter. *Ann. Bot.* **2002**, *89*, 895–905. [[CrossRef](#)] [[PubMed](#)]
92. Oren, R.; Sperry, J.S.; Katul, G.; Pataki, D.E.; Ewers, B.; Phillips, N.; Schäfer, K. Survey and synthesis of intra-and interspecific variation in stomatal sensitivity to vapour pressure deficit. *Plant Cell Environ.* **1999**, *22*, 1515–1526. [[CrossRef](#)]
93. Bowman, W.D. The relationship between leaf water status, gas exchange, and spectral reflectance in cotton leaves. *Remote Sens. Environ.* **1989**, *30*, 249–255. [[CrossRef](#)]
94. Maas, S.; Dunlap, J. Reflectance, transmittance, and absorptance of light by normal, etiolated, and albino corn leaves. *Agron. J.* **1989**, *81*, 105–110. [[CrossRef](#)]
95. Adams, M.L.; Philpot, W.D.; Norvell, W.A. Yellowness index: An application of spectral second derivatives to estimate chlorosis of leaves in stressed vegetation. *Int. J. Remote Sens.* **1999**, *20*, 3663–3675. [[CrossRef](#)]
96. Globe, D. *The Benefits of the 8 Spectral Bands of Worldview-2*; White Paper; Digital Globe: Westminster, CO, USA, 2009; Volume 12.
97. Zengeya, F.M.; Mutanga, O.; Murwira, A. Linking remotely sensed forage quality estimates from worldview-2 multispectral data with cattle distribution in a savanna landscape. *Int. J. Appl. Earth Obs. Geoinform.* **2013**, *21*, 513–524. [[CrossRef](#)]
98. McMurtrey, J.; Chappelle, E.; Kim, M.; Meisinger, J.; Corp, L. Distinguishing nitrogen fertilization levels in field corn (*Zea mays* L.) with actively induced fluorescence and passive reflectance measurements. *Remote Sens. Environ.* **1994**, *47*, 36–44. [[CrossRef](#)]
99. Yoder, B.J.; Waring, R.H. The normalized difference vegetation index of small douglas-fir canopies with varying chlorophyll concentrations. *Remote Sens. Environ.* **1994**, *49*, 81–91. [[CrossRef](#)]
100. Buschmann, C.; Langsdorf, G.; Lichtenthaler, H. Imaging of the blue, green, and red fluorescence emission of plants: An overview. *Photosynthetica* **2001**, *38*, 483–491. [[CrossRef](#)]
101. Papageorgiou, G.C. *Chlorophyll A Fluorescence: A Signature of Photosynthesis*; Springer Science & Business Media: Berlin, Germany, 2007; Volume 19.
102. Gitelson, A.A.; Buschmann, C.; Lichtenthaler, H.K. Leaf chlorophyll fluorescence corrected for re-absorption by means of absorption and reflectance measurements. *J. Plant Physiol.* **1998**, *152*, 283–296. [[CrossRef](#)]
103. Lichtenthaler, H.; Wenzel, O.; Buschmann, C.; Gitelson, A. Plant stress detection by reflectance and fluorescence. *Ann. N. Y. Acad. Sci.* **1998**, *851*, 271–285. [[CrossRef](#)]
104. Demmig-Adams, B.; Adams, W.W. The role of xanthophyll cycle carotenoids in the protection of photosynthesis. *Trends Plant Sci.* **1996**, *1*, 21–26. [[CrossRef](#)]
105. Flexas, J.; Escalona, J.; Medrano, H. Water stress induces different levels of photosynthesis and electron transport rate regulation in grapevines. *Plant Cell Environ.* **1999**, *22*, 39–48. [[CrossRef](#)]
106. Gamon, J.A.; Serrano, L.; Surfus, J.S. The photochemical reflectance index: An optical indicator of photosynthetic radiation use efficiency across species, functional types, and nutrient levels. *Oecologia* **1997**, *112*, 492–501. [[CrossRef](#)] [[PubMed](#)]
107. Penuelas, J.; Filella, I.; Gamon, J.A. Assessment of photosynthetic radiation-use efficiency with spectral reflectance. *New Phytol.* **1995**, *131*, 291–296. [[CrossRef](#)]

108. Wong, C.; Gamon, J.A. Three causes of variation in the photochemical reflectance index (pri) in evergreen conifers. *New Phytol.* **2015**, *206*, 187–195. [[CrossRef](#)] [[PubMed](#)]
109. Hilker, T.; Coops, N.C.; Hall, F.G.; Black, T.A.; Wulder, M.A.; Nesic, Z.; Krishnan, P. Separating physiologically and directionally induced changes in pri using brdf models. *Remote Sens. Environ.* **2008**, *112*, 2777–2788. [[CrossRef](#)]
110. Barton, C.; North, P. Remote sensing of canopy light use efficiency using the photochemical reflectance index: Model and sensitivity analysis. *Remote Sens. Environ.* **2001**, *78*, 264–273. [[CrossRef](#)]
111. Evans, J.R. The allocation of protein nitrogen in the photosynthetic apparatus: Costs, consequences and control. In *Photosynthesis*; Alan R. Liss Inc.: New York, NY, USA, 1989; pp. 183–205.
112. Inoue, Y.; Guérif, M.; Baret, F.; Skidmore, A.; Gitelson, A.; Schlerf, M.; Darvishzadeh, R.; Oliso, A. Simple and robust methods for remote sensing of canopy chlorophyll content: A comparative analysis of hyperspectral data for different types of vegetation. *Plant Cell Environ.* **2016**, *39*, 2609–2623. [[CrossRef](#)] [[PubMed](#)]
113. Atzberger, C.; Guérif, M.; Baret, F.; Werner, W. Comparative analysis of three chemometric techniques for the spectroradiometric assessment of canopy chlorophyll content in winter wheat. *Comput. Electron. Agric.* **2010**, *73*, 165–173. [[CrossRef](#)]
114. Hansen, P.; Schjoerring, J. Reflectance measurement of canopy biomass and nitrogen status in wheat crops using normalized difference vegetation indices and partial least squares regression. *Remote Sens. Environ.* **2003**, *86*, 542–553. [[CrossRef](#)]
115. Ali, I.; Greifeneder, F.; Stamenkovic, J.; Neumann, M.; Notarnicola, C. Review of machine learning approaches for biomass and soil moisture retrievals from remote sensing data. *Remote Sens.* **2015**, *7*, 16398–16421. [[CrossRef](#)]
116. Doktor, D.; Lausch, A.; Spengler, D.; Thurner, M. Extraction of plant physiological status from hyperspectral signatures using machine learning methods. *Remote Sens.* **2014**, *6*, 12247–12274. [[CrossRef](#)]



© 2017 by the authors. Licensee MDPI, Basel, Switzerland. This article is an open access article distributed under the terms and conditions of the Creative Commons Attribution (CC BY) license (<http://creativecommons.org/licenses/by/4.0/>).